Available online at www.sciencedirect.com
SCIENCE DIRECT
Polymer 46 (2005) 1295–1308
polymer
www.elsevier.com/locate/polymer

The effect of the polymerization route on the amount of interphase in structured latex particles and their corresponding films

Didier Colombini[b,1], Nadia Ljungberg[a,2], Helen Hassander[a,3], Ola J. Karlsson[a,*]

[a]Department of Polymer Science and Engineering, Lund University, P.O. Box 124, SE-221 00 Lund, Sweden
[b]Fibre Science and Communication Network, Mid Sweden University, SE-851 70 Sundsvall, Sweden

Accepted 30 September 2004
Available online 8 December 2004

Abstract

Three series of hard/soft styrene–acrylic latex based systems with equivalent compositions were prepared either by blending of homopolymer latexes or by preparing structured latex particles having core shell (CS) or inverted core shell (ICS) morphologies. Transmission electron microscopy (TEM) was used to investigate the particle morphologies, which were correlated to the calculated fractional radical penetration for the propagating species during the reactions. The thermo-mechanical properties as well as the morphology of the resulting latex films were analyzed by differential scanning calorimetry (DSC), dynamic mechanical analysis (DMA) and TEM. The viscoelastic properties of the interphase between the first and second-stage polymers formed in the structured hard/soft latex films, as well as its qualitative amount and also the film morphologies were found to depend on the interplay between thermodynamic and kinetic parameters during the synthesis of the samples.

Keywords: Core shell latex particles; Latex blends; Interphase

1. Introduction

The process of film formation from latex dispersions underlies much of the technology of water-borne coatings and there is a need for sufficient understanding to permit the development of high performance coatings that are environmentally friendly. A major difficulty which is associated with water-based coatings arises from the competition between film formation and mechanical film properties [1–3]. For example, low-glass-transition-temperature (T_g) polymer-based latexes have good film forming abilities but lead to poor mechanical film properties upon the evaporation of water, and are thus not sufficient enough to function in modern coatings.

It is well known that the mechanical behavior of multiphase polymer materials is governed by many separate parameters e.g. the mechanical properties of the neat constituents, the morphology, the interfacial activity between the phases and the blend composition [4–7]. Therefore, several approaches have been explored to overcome the lack of mechanical strength in low-T_g polymer based latexes. One solution is the use of structured core/shell latex particles [8–11] that have a high-T_g polymer core and a low-T_g film-forming polymer shell. The corresponding dry films have been described [8–13] as equivalent to elastomeric matrices containing rigid inclusions. Another way to significantly enhance the mechanical properties of soft latex films is achieved by physically blending two separate polymer dispersions with homogeneous particle morphologies. Thus, the combination of soft (i.e. low-T_g) and hard (i.e. high-T_g) latexes has become an area of specific scientific and technical interests resulting, in the last few years, in numerous publications

* Corresponding author. Tel.: +46 706 30 85 74; fax: +46 46 222 41 15.
E-mail addresses: didier.colombini@ggbearings.com (D. Colombini), nadia.ljungberg@cermav.cnrs.fr (N. Ljungberg), helen.hassander@polymer.lth.se (H. Hassander), ola.karlsson@polymer.lth.se (O.J. Karlsson).
[1] GGB R and D, P.O. Box 2074, F-74009 Annecy Cedex, France. Tel.: +33 4 50 33 66 76.
[2] CERMAV, P.O. Box 53, F-38041 Grenoble Cedex 9, France. Tel.: +33 4 76 03 76 08.
[3] Tel.: +46 46 222 06 22.

0032-3861/$ - see front matter © 2004 Elsevier Ltd. All rights reserved.
doi:10.1016/j.polymer.2004.11.056

[1,3,10,12–39] on film formation and mechanical film properties of blends of polymer dispersions.

Among other techniques, differential scanning calorimetry (DSC) and dynamic mechanical analysis (DMA) have been successfully used to characterize and to provide relevant information on multiphase polymeric materials [4–7,40,41]. The key factor of a two-phase system in a DSC (or DMA) thermogram is the existence of two separate glass transitions (or associated α-relaxations, in the case of DMA) having temperature locations coinciding with those of the pure constituents. Subsequently the changes in these transition temperatures in comparison with those measured for the neat constituents are often discussed as reflecting chemical, physical and/or mechanical interactions between the phases [4–7,40,42–44].

Several publications have reported on theoretical calculations of the kinetics of emulsion polymerization reactions as well as of the development of the latex particle morphologies over the course of the reaction [45–54]. It is now established that the two main factors in the formation of a certain latex particle morphology are the drive for thermodynamic equilibrium [55–57] and/or the diffusivity of the propagating radicals [50,54,58–63]. Recent review articles covering many of the aspects involved in the variations in the morphology of structured latex particles are available [64–67]. Basically, thermodynamic equilibrium latex particle morphologies are achieved when the rate of diffusion of the polymer chain is much faster than the polymerization rate, whereas the kinetically controlled latex particle morphologies are obtained when the diffusion rate and/or the phase separation are slower than the polymerization rate of the second-stage polymer. However, this is a simplified description and the full analysis to this complicated subject is much more diversified.

In the present work, three series of non-polar hard and polar soft styrene–acrylic latex based systems with identical compositions (i.e. hard/soft ratios of 40:60 by weight) were prepared either by blending of the homo polymer latexes or by preparing structured latex particles having core shell (CS) or inverted core shell (ICS) morphologies. By associating their particle and film morphologies as well as their thermo-mechanical film properties with polymerization kinetics calculations, it was aimed to investigate the dependence of the polymerization route on the interfacial properties of the hard/soft latex based materials.

2. Sample preparation and characterization

2.1. Materials

Methyl methacrylate (MMA), styrene (S), butyl acrylate (BuA), and methacrylic acid (MAA) were supplied by Merck and used as received. Sodium persulfate (NaPS) and sodium dodecyl sulfate (SDS), also from Merck, were of analytical grade and used without further treatment. All other chemicals were used as supplied.

2.2. Latex preparation—emulsion polymerization

The emulsion polymerizations were performed in a 1-L, four-necked glass reactor equipped with a mechanical stirrer, a reflux condenser, and a thermometer. The reactor was immersed in a thermostatic water-bath in order to maintain a reaction temperature of 70 ± 0.5 °C. Three homogeneous latexes were polymerized in single-stage polymerizations and four hard/soft structured latexes, were prepared in two-stage polymerization processes. The structured latexes were defined as either core-shell (CS) or inverted core-shell (ICS) depending on in what order the reactor had been charged, but common for them all was that the stage ratio between the hard, high-T_g polymer and the soft, low-T_g polymer was 40:60 (by weight). Details for the polymerizations are given in Table 1.

For all experiments, 155 g of deionized water was added to the reactor, which was then purged with nitrogen. When the reactor temperature was stable at 70 °C charging of the initiator and the monomer emulsions was started. For the homogeneous latexes, 25 g of Emulsion-1 together with Init-1 were pre-charged to the reactor and the remaining amount of Emulsion-1 together with Init-2 were continuously added during 4.5 h.

The CS-series consisted of a non-polar, hard, first-stage polymer, poly(styrene-*co*-butyl acrylate), p(S-*co*-BuA), and a polar, soft, second-stage polymer, poly(methyl methacrylate-*co*-butyl acrylate-*co*-methacrylic acid), p(MMA-*co*-BuA-*co*-MAA). The p(S-*co*-BuA) had a T_g of either 60 or 80 °C and the p(MMA-*co*-BuA-*co*-MAA) had a T_g of 20 °C. For the preparation of the CS latexes the reactor was charged with 10 g of Emulsion-1 along with Init-1 and after 15 min a continuous feeding of Emulsion-1 and Init-2 was started. The total addition time of Emulsion-1 was 110 min and for Init-2 the feeding period lasted for 130 min. One hour after all of Emulsion-1 had been added charging of Emulsion-2 together with Init-2 began. Emulsion-2 was continuously fed for 160 min, while Init-2 was added for another 180 min.

Inversely, the ICS series consisted of the polar p(MMA-*co*-BuA-*co*-MAA) as the first-stage polymer and the non-polar p(S-*co*-BuA) as the second-stage polymer (Table 1). In these experiments the reactor was pre-charged with 15 g of Emulsion-1 along with Init-1. After 15 min the remaining amount of Emulsion-1 was fed for 160 min and Init-2 was continuously fed to the reactor for 180 min. One hour after all of Emulsion-1 had been added, charging of Emulsion-2 and Init-2 was started. The feed time for Emulsion-2 was 110 min and for the remaining Init-2, 130 min. Independent of the polymerization method, the reactor temperature was kept at 70 °C for 30 min after all the monomer and initiator had been added. Subsequently, the reactor was cooled to room temperature.

Table 1
Sample codes, polymerization recipes, and detailed reaction conditions

Sample codes	Homogeneous latexes			Structured latexes			
	20SL	60HL	80HL	60CS20	60ICS20	80CS20	80ICS20
Reactor charge							
Water (g) 155	155	155	155	155	155	155	155
Emulsion-1							
Water (g)	352.6	331.6	331.6	141.1	211.5	141.1	211.5
NaOH (g)	0.3	0.3	0.3	0.12	0.18	0.12	0.18
SDS (g)	8.6	8.6	8.6	3.3	5.3	3.3	5.3
Styrene (g)	/	308.4	364.1	123.4	/	145.6	/
MMA (g)	227.6	/	/	/	132	/	132
BuA (g)	218.7	119.9	64.3	48	126	25.7	126
MAA (g)	12.9	/	/	/	7.7	/	7.7
Feed rate (g/h)	178	167	167	168	177	168	177
Init-1							
Water (g)	0.76	0.76	0.76	0.76	0.76	0.76	0.76
NaPS (g)	0.19	0.19	0.19	0.19	0.19	0.19	0.19
Emulsion-2							
Water (g)	/	/	/	211.5	141.1	211.5	141.1
NaOH (g)	/	/	/	0.2	0.12	0.2	0.12
SDS (g)	/	/	/	5.3	3.3	5.3	3.3
Styrene (g)	/	/	/	/	123.7	/	145.6
MMA (g)	/	/	/	132	/	132	/
BuA (g)	/	/	/	126	48	126	25.7
MAA (g)	/	/	/	7.7	/	7.7	/
Feed rate (g/h)	/	/	/	182	174	182	174
Init-2							
Water (g)	38	38	38	38	38	38	38
NaPS (g)	1.28	1.28	1.28	1.28	1.28	1.28	1.28

In addition, the homogeneous hard latexes (HL), with a T_g of either 60 or 80 °C, as well as the homogeneous soft latex (SL), with a T_g of 20 °C, that had been separately synthesized, were mixed to obtain the third series referred to as latex blend (LB), with a hard/soft weight ratio equivalent to that of the structured samples within the CS- and the ICS-series.

With respect to the T_g:s of the hard and the soft phases, samples that belonged to the CS-, to the ICS- or to the LB-series were denoted *60CS20* and *80CS20*, *60ICS20* and *80ICS20*, or *60LB20* and *80LB20*, respectively. Similarly, the homogeneous latexes were denoted with their respective T_g:s and the nature of the latex, i.e. *80HL*, *60HL* and *20SL* where HL represents hard latex and SL soft latex.

2.3. Sample characterization

2.3.1. Structured and homogeneous latex dispersions

Monomer conversion of the second-stage polymerization was monitored by gravimetry, measurements of the viscosity of the dispersions were carried out at room temperature using a Brookfield viscometer at 20 rpm (spindle 1), and particle sizes were obtained by laser diffraction using a Malvern Mastersizer 2000.

The minimum film formation temperature (MFT) was measured by using an MFT bridge (Coesfeld, Thermostair) with a temperature gradient covering either the range 0–32 °C or 28–60 °C in a static dry atmosphere. The dispersion samples that consisted of homogeneous or structured latexes were applied on metal foil with an application bar having a gap thickness of 200 μm. The MFT was defined as the crack-point temperature above which the dispersion formed a continuous film.

The final solids content of the dispersions was measured gravimetrically. Approximately 3 g of the dispersions was poured into test tubes and was allowed to dry overnight in an oven at 60 °C. The reported data corresponds to the average from a set of five measurements.

The latex particle morphologies were studied by means of transmission electron microscopy (TEM). A 5 ml portion of the dispersion, diluted to 0.1 wt% solids content, was negatively stained with a drop of an aqueous solution of 2% uranyl acetate (UAc). A drop of the resulting mixture was then placed on a formvar-coated grid and the water was removed by adsorption with a filter paper. The samples were examined in a Philips CM 10 transmission electron microscope. Micrographs were recorded on negative films, which were subsequently scanned. In the micrographs, the PS-rich phase appeared as dark and the MMA-*co*-BuA-rich phase as bright domains [68,69].

2.3.2. Homogeneous, structured and blended latex films

Films were prepared of the four structured latexes, the two latex blends and the homogeneous soft latex by casting

4 g of the dispersions on Petri dishes with surface areas of ~40 cm^2. The dishes were then placed in a conventional oven at 42 °C and the dispersions were covered with inverted Petri dishes in order to slow down the film formation process. After 48 h, the formed films had thicknesses of ~ 400 μm. The homogeneous, hard latexes could not form films, since their MFT:s were higher than 42 °C (Table 2) and thus became white powders when left in the oven to dry. In order to be able to characterize them by dynamic mechanical analysis, the *60HL* and *80HL* powders were placed in a mould between aluminum foils and heat-pressed at 180 °C for 8 min, followed by 2 min under 2.2 MPa pressure. Consequently, clear, hard films with a thickness of ~400 μm were obtained.

Differential Scanning Calorimetry (DSC) thermograms of the latex films were recorded using a TA Instruments DSC-Q1000 under a nitrogen atmosphere. The temperature was first jumped from room temperature to 150 °C, where it was maintained for 3 min. The samples were then cooled at 10 °C/min down to −70 °C. After a 3-minute equilibrium time at −70 °C, the samples were heated up to 180 °C with a heating rate of 10 °C/min. The sample weights were approximately 5 mg and the experiments were carried out in hermetically sealed pans.

The TA Instruments Dynamic Mechanical Analyzer DMA 2980 was used, operating in tensile mode under isochronal conditions at the frequency of 1 Hz, to measure the temperature dependence of the complex elastic modulus E^* (storage, E', and loss, E'', moduli) for the latex films. The samples were approximately 12 mm long, 5 mm wide and 400 μm thick. The viscoelastic spectra were recorded from −110 to 200 °C with a heating rate of 2 °C/min.

The Philips CM 10 transmission electron microscope was also used to investigate the morphology of the latex films. The samples were cut in an ultracryo-microtome Leica Ultracut T where the sample and knife temperatures were set at −70 and −40 °C, respectively. A solution of 50% DMSO in water was used as trough liquid and the sample thickness was 70 nm. All the sections were stained with ruthenium tetraoxide for 5 min (some samples were also stained before sectioning), and then examined in the transmission electron microscope. Micrographs were recorded on negative films, which were subsequently scanned. In the TEM micrographs the MMA-*co*-Sty phase appeared darker than the MMA-*co*-BuA phase domains [68,69].

3. Results

3.1. Properties of the latex dispersions—structured particle morphologies

A summary of the latex properties, including MFT:s and dispersion viscosities, is given in Table 2. It can be seen that all the latexes had solids contents of 44±1 wt% and the particle sizes were 125±25 nm. The structured latex particle morphologies were studied by means of TEM. Since the hard p(S-*co*-BuA) was more hydrophobic than the soft p(MMA-*co*-BuA-*co*-MAA), the expected thermodynamic equilibrium morphology for both the CS- and ICS-latexes should be core-shell with the hard, non-polar p(S-*co*-BuA) forming the core and the soft, more polar p(MMA-*co*-BuA-*co*-MAA) forming the shell. TEM micrographs of the heterogeneous latex particles can be seen in Fig. 1. Negative staining with uranyl acetate (UAc) was used in order to visualize whether the particles were film forming or not and the staining can be observed as thin dark rings around the particles. Since the styrene-rich phase is more stable to the electron beam [68,69], the micrographs portray the p(S-*co*-BuA) domains as dark whereas the p(MMA-*co*-BuA-*co*-MAA)-rich phase appeared much lighter. In Fig. 1(a), the *80CS20* particles appear as dark spheres having a faint thin shell, possibly consisting of lumps of p(MMA-*co*-BuA-*co*-MAA) on the outside of the seed particles but from only the whole particle TEM micrograph it is difficult to clearly tell the morphology [70]. Fig. 1(b)–(d) display the *80ICS20*, *60CS20* and *60ICS20* latexes, respectively, and similar particle morphologies were observed in these three experiments. No certain differences in latex particle morphologies could be seen between *60CS20*, *60ICS20* and *80ICS20* and the observed structures were close to the expected thermodynamic equilibrium non-polar core/polar shell morphology i.e., the

Table 2
Properties of the homogeneous and structured latex dispersions

T_g (°C)			MFT (°C)	solids content (wt%)	Viscosity (mPa s)	Particle size (nm)
	Stage 1	Stage 2				
80HL	76	/	>70	43	49	124
60HL	54	/	54±2	45	77	122
20SL	21	/	13±2	45	75	108
80CS20	76	30	37±2	44	15	150
60CS20	56	20	26±2	44	21	113
80ICS20	21	76	33±2	44	22	148
60ICS20	21	56	29±2	44	22	95
80LB20	17	76	18±2	44	n.a	n.a
60LB20	21	56	17±2	44	n.a	n.a

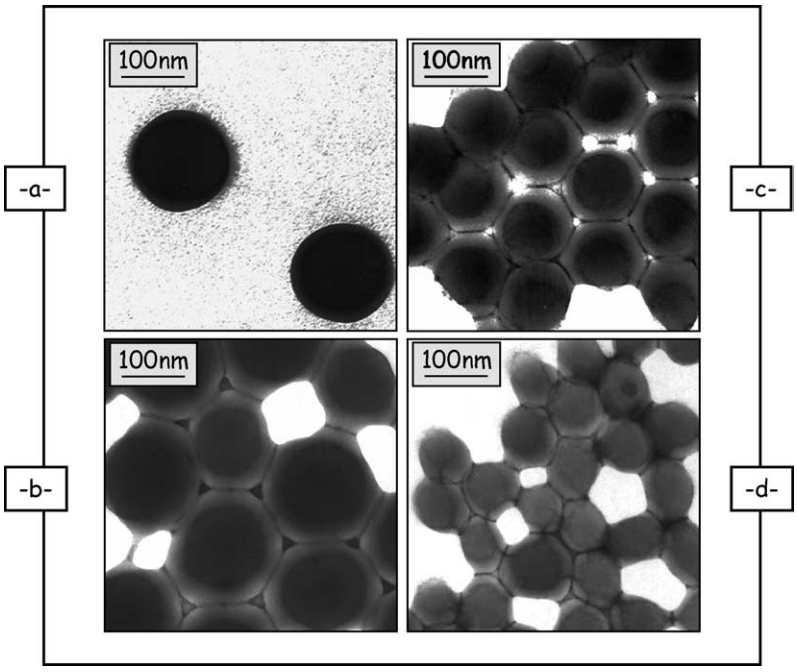

Fig. 1. TEM micrographs – Structured latex particle morphologies. a. 80CS20, b. 80ICS20, c. 60CS20, d. 60ICS20.

particle cores consisted of the high-T_g p(S-*co*-BuA), that was enclosed by the low-T_g p(MMA-*co*-BuA-*co*-MAA), which composed the shell.

3.2. Thermal, viscoelastic and morphological film properties

DMA, DSC and TEM were used to characterize thermo-mechanical and morphological film properties. Fig. 2 gives the thermal and mechanical viscoelastic film properties for the three homogeneous latexes; *80HL*, *60HL* and *20SL*. In Fig. 2(a) the $\partial\Delta C_p/\partial T$ obtained from DSC measurements is plotted as a function of temperature. The peak values correspond to the inflection point of the ΔC_p signal and thus represent the glass transition temperatures of the materials. Fig. 2(b) and (c) display the temperature dependencies of the storage modulus (E') and the loss factor tan δ, respectively, obtained from DMA measurements. The drop in storage modulus (Fig. 2(b)) reflects the α-relaxation which is associated with the glass transition of the material. Each tan δ spectrum (Fig. 2(c)) showed a peak reflecting the drop in E' when passing through the α-relaxational process. Since the tan δ is defined as the ratio between the loss and storage moduli $\left(\tan\delta = \frac{E'/}{E'}\right)$, the temperature location of the tan δ peak is slightly higher than that of the inflection point of the storage modulus.

Fig. 3 displays the heat capacity (ΔC_p) as a function of temperature for (a) the 80/20 group and (b) the 60/20 group (comprising the CS, ICS and LB samples as well as the homogeneous latexes). It can be seen in Fig. 3(a) that the *20SL* and *80HL* thermograms display jumps in ΔC_p at approximately 20 and 80 °C, respectively, corresponding to the T_g:s for the homogeneous latexes. In the blend, *80LB20*, it was clear that the two different latexes were not phase-mixed, since there were significant jumps in ΔC_p at the same temperature locations as for the homogeneous latexes. The CS and ICS samples, however, showed some broadening in the curves indicating the existence of interphase in these systems. The largest broadening was found for the *80CS20* sample, whilst the *80ICS20* curve resembled that of the latex blend.

Similar trends can be observed for the 60/20 group in Fig. 3(b). The trends are, however, slightly more difficult to distinguish as a result of the smaller temperature span between the T_g:s of the soft and hard phases as compared to the 80/20 group. Nevertheless, it was clear that the blend sample, *60LB20*, showed two distinct ΔC_p jumps that corresponded to those for the homogeneous latexes indicating that no phase mixing had occurred, whilst the CS and ICS samples showed broadening in the curves.

To further investigate the existence of interphase in the systems, thermal (DSC) and mechanical viscoelastic (DMA) properties of the film samples were examined. Fig. 4 displays the temperature dependence of (a) $\partial\Delta C_p/\partial T$, (b) E' and (c) tan δ, for the 80/20 group. For comparison with the homogeneous *20SL* and *80HL* films the temperature location of the maximum of $\partial\Delta C_p/\partial T$ and tan δ are recalled in Fig. 4(a) and (c), respectively. The corresponding curves for the 60/20 group can be seen in Fig. 5(a)–(c).

Fig. 4(a) clearly shows two separate $\partial\Delta C_p/\partial T$ peaks for the *80LB20* sample. Also *80ICS20* showed two separated peaks, but the distance between them was somewhat smaller as compared to the blend. The *80CS20* sample, however, displayed extensive broadening around its low temperature

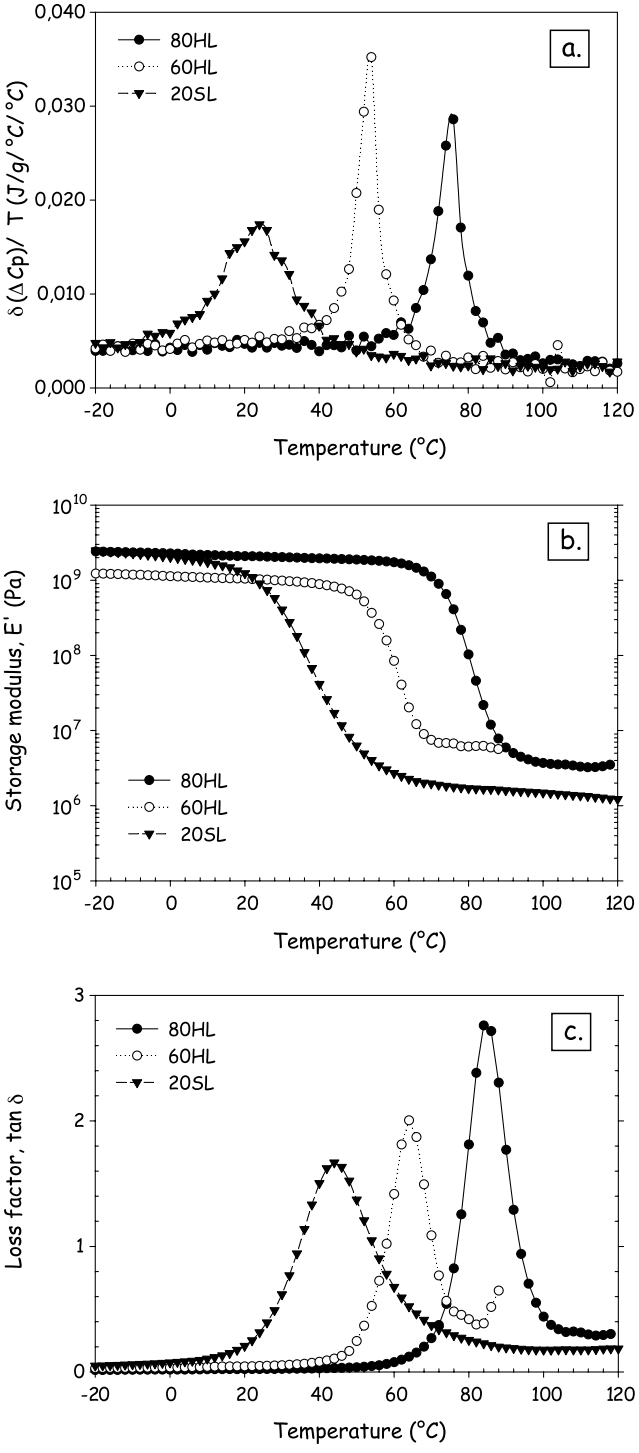

Fig. 2. Thermal (DSC) and mechanical viscoelastic (DMA, at 1 Hz) properties of the homogeneous latex films. $\partial\Delta C_p/\partial T$ *versus* temperature. b. Storage modulus (E′) *versus* temperature. c. Loss factor (tan δ) *versus* temperature.

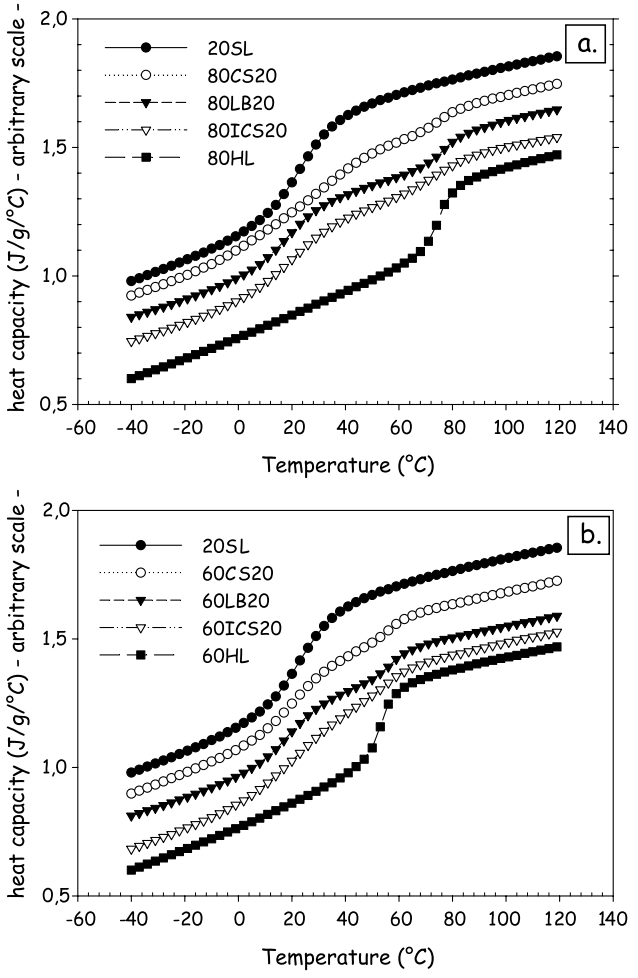

Fig. 3. DSC traces (heat capacity, ΔC_p) of the two latex samples series. High Tg 80°C series. High Tg 60°C series.

peak and the distance between the two peaks was significantly smaller.

In Fig. 4(b) the storage modulus is displayed as a function of temperature for the three bimodal 80/20 systems. It can be observed that at low temperatures (up to approximately 20 °C) the moduli were practically equivalent for all three samples. In the temperature span 30–60 °C, however, it can be seen that *80CS20* had a slightly higher modulus than *80ICS20* which in turn had a higher modulus than *80LB20*. When further increasing the temperature the order of the samples changed repeatedly during short temperature intervals and above 75 °C it was *80LB20* that had the highest modulus followed by *80ICS20* and *80CS20*.

It can also be observed in Fig. 4(b) that *80CS20* displayed a drop in storage modulus over a larger temperature span than the other two samples and that there was only a very small indication of a drop at high temperature. Consequently, the tan δ for *80CS20* in Fig. 4(c) displayed one large peak in between the two temperature locations for the tan δ of the homogeneous latexes but slightly closer to the low temperature peak. The latex blend displayed two separated tan δ peaks that corresponded well with the temperature locations for the maximum of the homogeneous latex peaks, thus further evidencing that no phase mixing occurred in the blend, while the peaks for *80ICS20* had approached each other as compared to the latex blend,

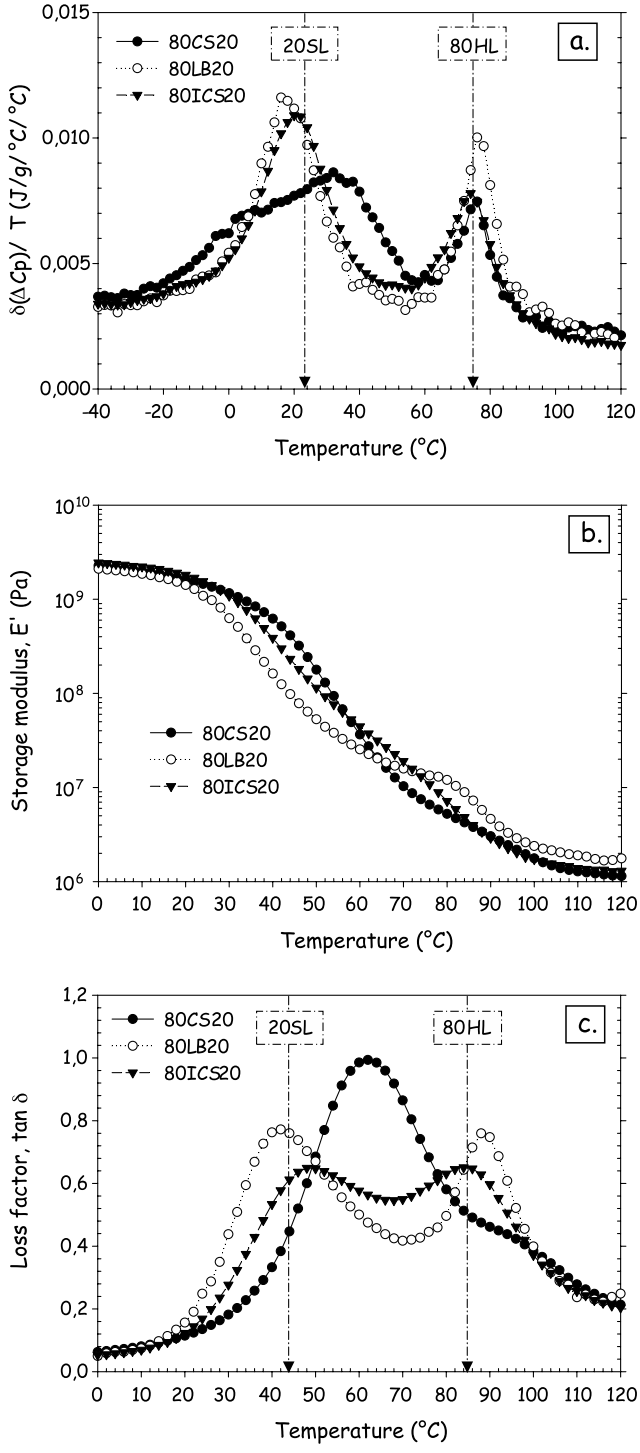

Fig. 4. Thermal (DSC) and mechanical viscoelastic (DMA) properties of the 80CS20, 80LB20, and 80ICS20 samples. $\partial\Delta C_p/\partial T$ *versus* temperature. Storage modulus (E′) *versus* temperature. Loss factor (tan δ) *versus* temperature. Two arrows recall (for comparison) the temperature location of the maximum of $\partial\Delta C_p/\partial T$ and tan δ recorded (DMA) for the homogenous 20SL and 80HL latex films.

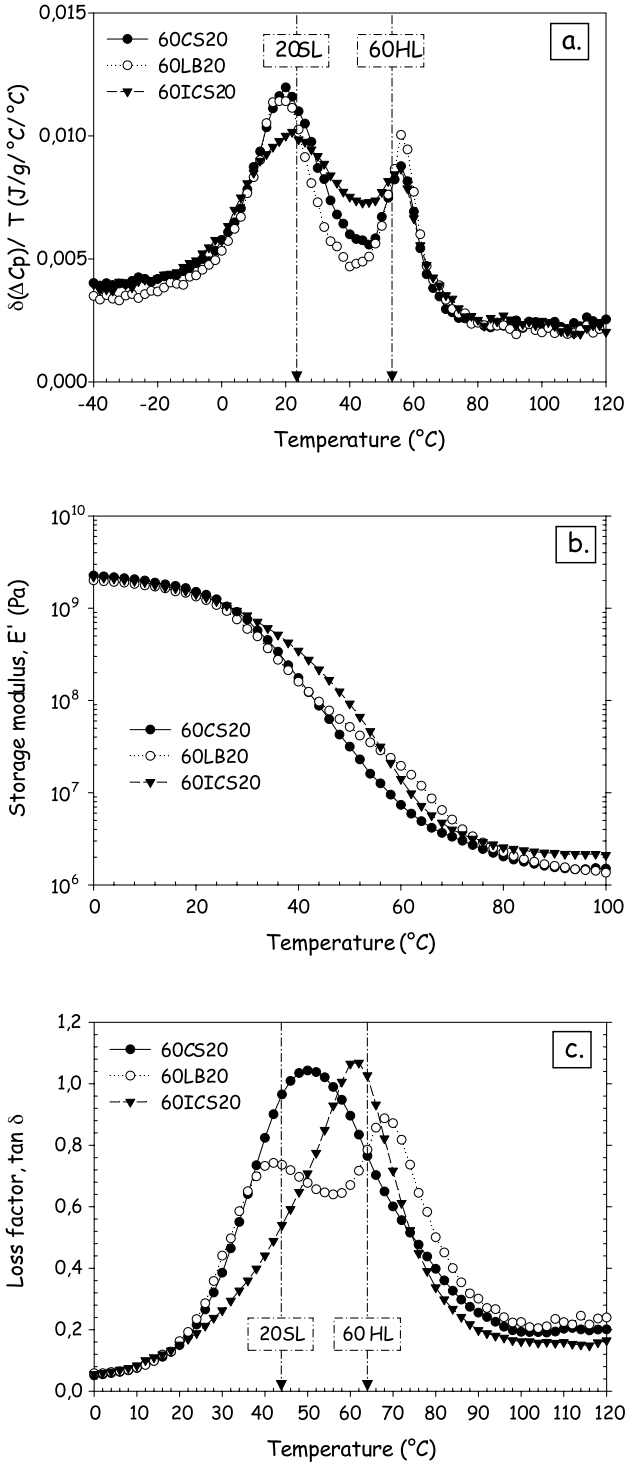

Fig. 5. Thermal (DSC) and mechanical viscoelastic (DMA) properties of the 60CS20, 60LB20, and 60ICS20 samples. $\partial\Delta C_p/\partial T$ *versus* temperature. Storage modulus (E′) *versus* temperature. Loss factor (tan δ) *versus* temperature. Two arrows recall (for comparison) the temperature location of the maximum of $\partial\Delta C_p/\partial T$ and tan δ recorded (DMA) for the homogeneous 20SL and 80 HL latex films.

giving rise to some overlapping. These observations strongly suggest a larger amount of interphase in the *80CS20* sample than in the other two bimodal systems within the 80/20 group.

Similar trends can be observed for the 60/20 group in Fig. 5, but are less clear because of the smaller temperature span between the T_g:s of the hard and soft phases. In Fig. 5(a) the latex blend is found to have two separated peaks, indicating no or very little phase mixing in the system, whereas the two other samples displayed broadening of the $\partial\Delta C_p/\partial T$ peaks. Fig. 5(b) clearly shows single drops in storage modulus for both *60CS20* and *60ICS20*, with the difference being the location of the inflection point. This behavior can be visualized even clearer in Fig. 5(c) where *60CS20* displayed a single peak shifted towards the temperature maximum of the soft, homogeneous latex and *60ICS20* showed a single peak closer to the temperature maximum of the hard, homogeneous latex. Thus there seemed to be a large amount of interphase present in the two structured samples compared to *60LB20*, with the interphase for *60CS20* being mainly soft and the interphase for *60ICS20* being mainly hard. As previously observed for the 80/20 group (Fig. 4(b)), Fig. 5(b) pointed out the temperature dependence of the moduli ratio of the samples (CS, ICS, LB) within the 60/20 group.

Fig. 6 shows TEM micrographs of the microtomed film samples (a) *80CS20*, (b) *80LB20*, (c) *80ICS20*, (d) *60CS20*, (e) *60LB20* and (f) *60ICS20*. Not surprisingly, it can be observed in Fig. 6(b) and (e) that the two films made from latex blends had morphologies indicating that no phase mixing occurred, thus confirming the interpretation of the thermal and viscoelastic mechanical data obtained by DSC and DMA. The domain sizes in the LB micrographs were consequently larger than in the micrographs (a) *80CS20*, (c) *80ICS20*, (d) *60CS20*, and (f) *60ICS20*. The larger domain size was due to the blending of whole particles of roughly 125 nm, whereas in the structured films the two co-polymers were confined within one latex particle as the starting point. The core-shell latexes *80CS20* (Fig. 6(a)) and *60CS20* (Fig. 6(d)) showed similar film morphologies where the second-stage p(MMA-*co*-BuA-*co*-MAA) was film forming and the first-stage p(S-*co*-BuA) core remained unaffected in the film. However, detailed studies of the p(S-*co*-BuA) core interior in the microtomed films, *80CS20* and *60CS20* indicated slight differences. In a majority of the studied first-stage polymer domains of *60CS20* there was only one small domain of second-stage p(MMA-*co*-BuA-*co*-MAA) observed. However, in the case of *80CS20* (Fig. 6(a)) there were several second-stage polymer domains visible in the first-stage polymer cores. In addition, it can be seen in Fig. 6(a) that the shape of the core domains in *80CS20* were not spherical in the microtomed films. This reflected an artifact created by the microtome knife, which compressed the particles in the direction of the cut. The films based on the *80ICS20* and *60ICS20* latexes also had similar morphologies with respect to each other. However, when the ICS based films (Fig. 6(c) and (f)) were compared to the CS based films (Fig. 6(a) and (d)) there was an obvious difference in the domain sizes of the p(S-*co*-BuA) phase, which in the ICS samples were much smaller than in the CS based films. Even though the TEM micrographs of the whole particles were found rather similar (Fig. 1), showing the p(S-*co*-BuA) forming, as it seemed, a homogeneous particle core it became clear while the resulting films were studied that there must have been a significant difference in the build-up mechanism of the polymer domains and accordingly also in the interphase structures in the CS and ICS latex particles. These differences will be further discussed in the next section by combining the results from the thermo-mechanical and morphological studies of the films with the polymerization kinetics.

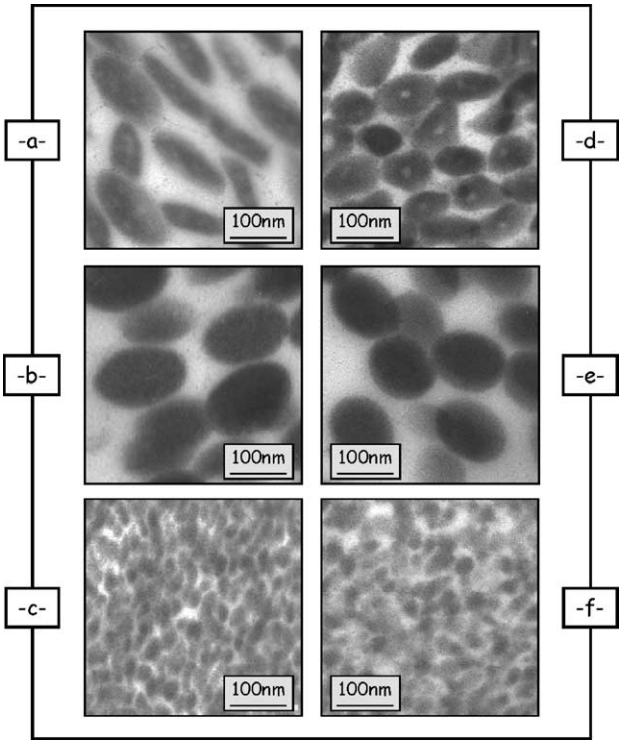

Fig. 6. TEM micrographs – Latex film morphologies. a. 80CS20, b. 80LB20, c. 80ICS20, d. 60CS20, e. 60LB20, F. 60ICS20.

4. Polymerization kinetics and fractional radical penetration

As mentioned earlier, the thermodynamic equilibrium latex particle morphology for the structured latexes based on polar p(MMA-*co*-BuA-*co*-MAA) and non-polar p(S-*co*-BuA) is likely to be a core-shell-type morphology involving a non-polar, hard core surrounded by a more polar, soft shell. The probability for the thermodynamic equilibrium morphology to be attained is dependent on a number of parameters, such as the polymer stage, the diffusivity in the

particle or the polarities of both the incoming radical and the polymer where it terminates. Practically, the polymerization kinetics can be assessed from a polymerization experiment and the knowledge of them permits for the extraction of data of particular interest for the interpretation of how the structural build-up in heterogeneous latexes proceeds. Sundberg et al. have recently proposed a considerable theoretical apparatus that has proven to be useful for the studies of the morphological evolution of structured latex particles over the course of the polymerizations [50,53,54,71,72]. The theoretical model has been tested and several papers are available describing its use in various experimental systems [73–76]. However, for a clearer understanding of the present study, a short presentation of the theoretical approach is required.

4.1. Radical fractional penetration model

The model is based on a few fundamental assumptions where the diffusion rates of the monomer and the growing radicals in the latex particles are of paramount importance for the kinetic evolution of the latex particle structures. It is assumed that the radicals are formed in the aqueous phase and that the oligo-radicals, which enter the particles unimpededly, diffuse and continue to grow by the addition of monomers to the polymer chain inside the particles. Eventually the radicals terminate and form second-stage domains [48,50]; the rate of termination being dependent on the relative diffusion rates of the two radicals involved in a particular termination reaction. However, in order to estimate the level of radical penetration in a latex particle, values for the diffusion coefficients of the radical species under the actual polymerization conditions are required. The monomer diffusion rates can be determined from a combination of the reaction temperature, the T_g of the polymer and the concentration of free monomer in the latex particles [71]. The diffusion coefficients for the radical species are, in addition to the diffusivity of small molecules in the polymer matrix, also to a large extent dependent on the chain length of the diffusing radical [50,54,77–79]. Furthermore, it is important to know the rate of the radical chain length increase [48,50,80,81].

In the present study:

- the polymerization propagation rate coefficients, k_p, and the termination rate coefficients, k_t, were calculated by anticipating that pseudo-bulk kinetics were valid at the high instantaneous monomer conversion prevailing [51,52,54,66,70,80–83],
- the diffusion rates for long and short radicals were calculated by taking into account the so-called ‘short long’ approximation, which states that a majority of the termination events involve a relatively short, mobile chain and a longer entangled one [80]. Thus in our calculations one of the radicals was always long, while the other one had a maximum length of 30 monomer units.

By combining diffusion rates, literature data for the used coefficients and the data extracted from the polymerizations, the life-time of a radical, t_r, under prevailing conditions could be expressed as

$$t_r = 1/k_t[R]$$

where $[R]$ is the radical concentration [50].

Finally, the radical life-time, t_r, and the diffusion rates for a growing radical were used to estimate the fractional penetration ratio, FP, which is defined as the distance a radical can penetrate into a particle divided by the particle radius [50]. An FP value lower than unity indicates the existence of diffusional restrictions preventing the growing radicals from penetrating the latex particles before termination occurs, which results in the formation of the second-stage polymer domains in the outer regions of the particle. On the other hand, a greater FP value indicates that the radicals are able to fully penetrate the particles. The FP concept was first derived for a polar first-stage polymer and a non-polar second-stage polymer, which would have an inverted core-shell morphology at thermodynamic equilibrium [50]. Later, a simplified FP concept was used on the reversed polymer system i.e., a non-polar seed and a polar second-stage polymer, which would ideally have a core-shell morphology [70]. The simplified version, which is also used in this work, categorizes the radical penetration depth into three classes based on the calculated diffusion rates and the average rate coefficients together with the estimated radical life-times. Subsequently, Class 1 allows full penetration, Class 2 partial penetration and Class 3 very limited penetration of the radicals.

In the present study, we have used both a non-polar first-stage polymer (np1) in combination with a polar second-stage polymer (p2) as well as the reversed case i.e., the same polymers in a different order of polymerization (p1/np2). The thermodynamic equilibrium morphologies for the np1/p2 and p1/np2 are then CS and ICS, respectively. A polar radical (p2) entering a non-polar polymer particle (np1) would end up on the outside of the non-polar polymer provided there were no diffusional restrictions in the polymers. However, if there were diffusional restrictions, which there could be in many seeded emulsion polymerizations or at high conversion, the second-stage polymer could be hindered to form the thermodynamic equilibrium morphology.

4.2. Application of the model

Table 3 reports the experimentally determined monomer concentrations in the particles, $[M]_p$, together with the calculated kinetic coefficients, k_t, k_p and t_r, the monomer

Table 3
Calculated kinetic coefficients and experimental parameters used

	$[M]_p$ (mol l^{-1})	D_M (cm^2 s^{-1})	k_p (l mol^{-1} s^{-1})	k_t (l mol^{-1} s^{-1})	t_r (s)	FP
60CS20	0.1	1.5×10^{-10}	14000	4.0×10^{3}	50	2
80CS20	0.1	1.9×10^{-12}	800	1.0×10^{3}	80	2
80ICS20-'exp'	1.1	1.5×10^{-6}	5300	1.2×10^{7}	0.7	1
80ICS20-'theo'	0.1	1.8×10^{-10}	5000	4.7×10^{3}	60	?
60ICS20-'exp'	0.6	1.1×10^{-6}	9700	8.9×10^{6}	0.9	1
60ICS20-'theo'	0.1	1.6×10^{-10}	8600	4.0×10^{3}	60	?

diffusion rates D_M and the estimated FP values for the CS- and ICS-series.

In the case of the CS-series, the presented values correspond to averages over the whole course of monomer feeding during the second-stage. The calculations were based on that an incoming radical in the second-stage polymerization entered the first-stage polymer and the diffusion rate used was based on the T_g of the first-stage polymer. This was a reasonable initial assumption but as the second-stage polymerization proceeded, new second-stage polymer domains were formed with other properties compared to the first-stage polymer. The radicals generated late in the second-stage could therefore enter another type of environment as compared to the radicals entering the particles early in the second-stage. In the calculation of t_r the possible change of radical environment was not taken into consideration for the CS-series.

For the ICS-samples, two values are presented for each experiment (Table 3). The calculated values *60ICS20*-'exp' and *80ICS20*-'exp' were based on samples withdrawn early in the second-stage polymerizations, where there was an initial monomer build-up. These calculations took into account the diffusivity in the first-stage polymer at the prevailing reaction conditions. Later in the reactions the monomer concentration, $[M]_p$, decreased and the average value for $[M]_p$ was in these polymerizations close to 0.1 mol/l (i.e. equivalent to that observed for the CS-series), which was used in the second set of values for the ICS-polymerizations i.e. *60ICS20*-'theo' and *80ICS20*-'theo'. The kinetic values reported for the *60ICS20*-'theo' and *80ICS20*-'theo' were calculated for second-stage radicals that polymerized and terminated inside already formed domains of second-stage polymer. This led to low diffusion rates of the monomer, D_M, and, therefore, to low values for the termination rate coefficients, k_t, and long radical life-times, t_r. In these calculations there was no significant effect on the values for the polymerization propagation coefficients, k_p, but in respect to D_M, t_r and k_t the resulting values were also comparable to the initial conditions in the second-stage of the CS-polymerizations. In addition, the ICS-'exp' values showed that the diffusivity in the first-stage low-T_g polymer was high in the ICS experiments. The diffusivity in the second-stage polymer would also be high late in the second-stage of the CS polymerizations where the low T_g second-stage polymer had formed a shell (Fig. 1(a) and (c)) and the incoming radicals would be less restricted but also have much less t_r than the estimated average values for the CS experiments reported in Table 3.

5. Discussion

In order to further discuss the differences between the samples it was deemed of interest to associate the experimental results from the thermo-mechanical and morphological studies of the films with the calculations related to the polymerization kinetics of the latex particles.

Based on the kinetic calculations, the CS-samples were assessed to belong to Class 2 having partial radical penetration of the high-T_g first-stage particles [70]. The Class 2 assessment was justified by the long life-times that indicated low termination rates and the low diffusion rates of the radicals in the first-stage polymer, which on average resulted in penetration distances shorter than the particle radius. In addition, the MFT values (Table 2) for these two samples were found to be higher than the second-stage T_g, which further indicated that fractions of the low-T_g polar second-stage oligo-radicals had penetrated into the existing particles and that the resulting polymer inside the first-stage particles were not able to participate in the film formation process. This was also observed in the TEM micrographs showing the film morphologies and cross-sections of the particles (Fig. 6(a) and (d)) where the non-polar first-stage polymer (np1) had small domains of polar second-stage polymer (p2) inside, indicating that the p2 radicals penetrated the np1, where they terminated and remained. In accordance with the higher calculated diffusion rates in *60CS20* as compared to *80CS20*, more domains of second-stage polymer inside the first-stage polymer were observed in the TEM micrograph of the *80CS20* sample. Finally, the thermo-mechanical analysis of the CS-series (Figs. 4 and 5) pointed out that a significant fraction of the second-stage polymer was participating in the interphase, thus resulting in the shift of the transition peak for the second-stage polymer towards that of the first-stage polymer.

The ICS-samples were initially considered to belong to Class 1 with full radical penetration of the low-T_g first-stage polymer because of their rather high k_p and k_t values and their short radical life-times. A significant diffusion of dead polymer chains would suggest that the morphology would be controlled by thermodynamic driving forces, and the equilibrium morphology based on minimization of the

interfacial energies should be considered. This was also what was observed in the TEM micrographs for these experiments. CS particle morphologies were observed in Fig. 1(b) and (d) but from the whole particle micrographs it was impossible to observe the internal particle structures that were revealed in Fig. 6(c) and (f) for the ICS-particle based films. The thermo-mechanical analysis confirmed that there were two distinct phases present (Figs. 3–5) but the rather high MFT values (Table 2) indicated that not all of the low-T_g polymer was participating in the film formation. In the *60ICS20* and *80ICS20* samples the non-polar second-stage polymer (np2) had no diffusional restrictions and could unhindered enter the polar first-stage polymer (p1) and form the domains of np2 inside p1. However, as the polymerization proceeded the radicals could be captured in the high-T_g np2 domains and possibly continue to grow in their own phase. The calculated kinetic coefficients for the reactions based on the second-stage polymer T_g differed significantly from the ones based on the first-stage polymer T_g (Table 3) and due to the diffusional restrictions and long t_r in the second-stage polymer late in the reactions, there were indications that there may have been phase-mixing and grafting onto existing polymer also in these experiments, which also was observed in the thermo-mechanical spectras as a shift of the α-relaxation (Figs. 4(c) and 5(c)).

The homogeneous single-stage latexes and the latex blends can be used as reference materials and from a reaction kinetic point of view they represent experiments with no radical penetration i.e., experiments that belong to Class 3. The small differences between the homogeneous neat latexes and the latex blends observed in the thermo-mechanical analysis reflected the minimum amount of interphase in these latex systems due to interparticle polymer diffusion that occurred during film formation. Consistently, their MFT values of 17 °C (60LB20) and 18 °C (80LB20) were found to be close to that of the soft phase, which supported the suggestion that the latex blend films had no (or very little) interfacial mixing as compared to the films made from the CS- and the ICS-dispersions.

When the radicals are long-lived the probability of grafting onto existing polymers via chain transfer to polymer increases during the late stages of a batch polymerization, or when the monomer is starve-fed. Lovell et al. [84–86] showed that the probability of a propagating chain undergoing transfer to polymer rather than propagation increased with an increase of either of the two ratios, k_{trP}/k_p and $[P]/[M]_p$, where [P] is the concentration of the repeating unit of the polymer and k_{trP} is the chain transfer to polymer rate coefficient [84, 87,88]. Since the $[P]/[M]_p$ ratio was kept high in all our experiments (apart from an initial monomer build-up in the ICS experiments) it was likely that chain transfer to the first-stage polymer occurred to a certain extent in all experiments. For *80CS20*, the large amount of interphase observed in the thermo-mechanical analysis could also, at least partly, be ascribed to grafting due to the lowering of k_p and, therefore, an increase in the k_{trP}/k_p ratio. When the calculations for the *80ICS20*-'theo' were performed no large effect on k_p was observed which might explain why there was less interphase in this experiment as compared to the *80CS20* sample. However, the radical life-times were long as a result of the reduced termination rates in the glassy first-stage polymer in *80CS20* and when the calculations were compared to those for *80ICS20* the situation was much more complex than if variations in only one single parameter could explain the observed behavior. The complexity is further exemplified since no decrease of k_p was observed in the *60ICS20* and *60CS20* experiments and yet there were differences in the amount and type of interphases in these two samples. It was observed that the interphase for *60CS20* was mainly soft whereas the interphase for *60ICS20* was mainly hard in the thermo-mechanical analysis, which on the other hand can be explained by the reaction kinetics of the emulsion polymerizations. For the *60ICS20* latex the high-T_g polymer was formed in the second-stage of the polymerization and the high-T_g polymer grafted onto the soft first-stage polymer. The reverse situation was prevalent during the second-stage polymerization of *60CS20* where the second-stage low-T_g polymer would graft onto the existing first-stage high-T_g polymer thus dominating the interphase and leading to a soft appearance in comparison to the *60ICS20* experiment.

The large differences in the observed amount of interphase between the DMA and the DSC can be explained by the sample preparation. By preheating the samples to 150 °C in the DSC experiments the interphasial mixing originating from restricted diffusion was removed and the differences observed between the blends and the structured latexes most likely was due to grafted polymer, which was not affected by the sample treatment. All the structured latexes showed interphasial mixing when analysed by means of DMA but the DSC results differed. However, the amount of interphase in *80CS20*, which was greater than in any of the other experiments, was still large as observed in the DSC trace, which further strengthened the calculations that pointed to the high probability for grafting to occur.

The differences in film morphology in Fig. 6 between the CS and ICS do not correspond to the difference in the amount of interphase from the thermo-mechanical analysis and the earlier discussion has shown it is difficult to explain the differences using only the presented reaction kinetic parameters. However, in a recent paper [89], Stubbs et al. stated that in polymerizations having high diffusion rates for all of the reacting species the formation of second-stage material would proceed via nucleation and growth. On the other hand, in polymerizations where diffusional restrictions are prevailing the second-stage polymer phase separation could instead occur via spinodal decomposition [70,89]. This would then also lead to differences in the amount of

interphase that is formed in the particles since the polymer phase separation may be limited when the second-stage radicals are able to partially penetrate the seed particles under monomer starved conditions, which would also result in increased interphasial mixing. Initially, the *80CS20* second-stage polymerization can be described as the experiment having the most diffusional restrictions and according to Stubbs et al. [89] it would be likely that, at least during the initial period of the second-stage, the formation of second-stage material could occur through spinodal decomposition. In the ICS-polymerizations there were initially no diffusional restrictions and in these experiments the most likely phase separation mechanism would be nucleation and growth of second-stage polymer followed by phase consolidation to attain the thermodynamic equilibrium non-polar core/polar shell morphologies. However, the high T_g of the non-polar second-stage polymer prevented a complete phase consolidation into one single phase domain having no grain boundaries, which is observed in Fig. 6 in the films where the particle cores were divided into smaller domains during film formation.

6. Conclusions

The present study benefits from the overlap of several research topics and thus links together areas such as emulsion polymerization, including kinetic and thermodynamic aspects that govern the latex particle morphologies, film formation from bimodal latex dispersions as well as thermal, mechanical and morphological characterizations of the multipolymeric films containing quantitatively and/or qualitatively different interphasial volumes.

The structured hard/soft styrene–acrylic latexes were prepared by two-stage emulsion polymerizations at 70 °C, which were in between the T_g:s either 80 or 60 °C of the non-polar high-T_g p(S-*co*-BuA) phase. The polar p(MMA-*co*-BuA-*co*-MAA) phase with a low T_g of 20 °C was always soft at the reaction temperature and the resulting structured latexes were denoted either as core-shell (CS) or as inverted core-shell (ICS) depending on in which order the reactor had been charged. The TEM analysis of the whole particle morphologies revealed that the particle structures in all samples were CS, in which the core consisted of the non-polar p(S-*co*-BuA) and the shell was made up from the polar p(MMA-*co*-BuA-*co*-MAA). However, when microtomed sections of the films were analyzed by means of TEM large differences were observed between the samples. Hard p(S-*co*-BuA) spherical particles in a matrix of film formed from the soft p(MMA-*co*-BuA-*co*-MAA) were observed in the reference latex blends (LB) samples, which were obtained by mixing hard and soft homogeneous latexes with a hard/soft weight ratio equivalent to that of the CS and ICS structured samples. In the CS films the hard p(S-*co*-BuA) cores were observed in a matrix of film forming second-stage p(MMA-*co*-BuA-*co*-MAA). Inside of the p(S-*co*-BuA) cores small domains of p(MMA-*co*-BuA-*co*-MAA) were observed, whose presence could be explained by the fractional radical penetration calculations. The films based on the ICS-series, which had the soft p(MMA-*co*-BuA-*co*-MAA) as the first-stage polymer and p(S-*co*-BuA) as second-stage polymer, showed another film morphology in which the p(S-*co*-BuA) core was divided into smaller domains during the film formation process. This particle structure that gave rise to the small second-stage polymer domains in the films was attributed to the possible formation of the second-stage material via a nucleation and growth mechanism where the consolidation of the second-stage material was not complete due to its high T_g.

From a general point of view, both the amount and the nature of the interphase in the structured hard/soft latex systems were found to depend on the preparation route of the samples. The nature of the interphase between the first and second-stage polymers was clearly affected by the complex interplay between thermodynamic and kinetic parameters during the synthesis e.g. the mobility of the second-stage polymer chains at the synthesis temperature and/or the relative hydrophobicity and compatibility of the first-stage polymer and the second-stage monomers as well as the ability for grafting. This had a direct influence on the thermo-mechanical and morphological film properties of the samples.

The DSC traces and the DMA thermograms both pointed out that a much larger amount of interphase had been formed in the CS and ICS samples in comparison to those from the LB-series. However, due to the sample preparation there were differences in the amount of interphase observed with DSC and DMA, respectively. Since the DSC samples were heated above the T_g of the hard phase prior to analysis, the interphase that was formed during the polymerization phase separated back to its pure constituents. The differences that could still be observed in the DSC traces for the structured samples as compared to the LB samples were attributed to grafted material formed in the synthesis, which could not phase separate during DSC sample preparation. The DMA thermograms showed then both the grafted interphase and the kinetically formed interphase, where the largest amount of total interpahse was observed in the *80CS20* sample, which was also supported by the polymerization kinetic calculations. Furthermore, large amounts of interphase were observed for both the *60CS20* and the *60ICS20* samples but the nature of their interphases differed and was considered as mainly soft for *60CS20* and mainly hard for *60ICS20*. The origin of the interphase was attributed to the diffusivities of the growing radicals and their probabilities to graft onto the existing polymer as well as the prevailing phase separation mechanism.

Acknowledgements

The authors would like to thank Frida Karlsson at

Celanese Emulsions Norden AB (Perstorp, Sweden) for the MFT measurements, and Lina E. Karlsson, Lund University, Sweden and Donald C. Sundberg and Jeffery M. Stubbs, University of New Hampshire, NH, USA for valuable discussions. The VINNOVA and Industry sponsored Centre for Amphiphilic Polymers from Renewable Resources (Sweden) are gratefully acknowledged for the financial support of this work.

References

[1] Winnik MA, Feng JR. J Coat Technol 1996;68:39.
[2] Keddie JL. Mat Sci Eng Rep 1997;21:101.
[3] Steward PA, Hearn J, Wilkinson MC. Adv Colloid Interface Sci 2000; 86:195.
[4] Bohn L. In: Platzer NA, editor. Copolymers, polyblends and composites: a symposium, 1974. p. 66.
[5] Krause S. In: Paul DR, Newman S, editors. Polymer blends. New York: Academic Press; 1978. p. 15.
[6] Dickie RA. In: Paul DR, Newman S, editors. Polymer blends. New York: Academic Press; 1978. p. 353.
[7] Lipatov YS. Physical chemistry of filled polymers. London: British Library; 1979.
[8] Juhue D, Lang J. Macromolecules 1995;28:1306.
[9] Hagen R, Salmen L, Karlsson O, Wesslen B. J Appl Polym Sci 1996; 62:1067.
[10] Heuts MPJ, Le Fêbre RA, Van Hilst JLM, Overbeek GC. ACS Symp Ser 1996;648:271.
[11] Lepizzera S, Lhommeau C, Dilger G, Pith T, Lambla M. J Polym Sci, Part B: Polym Phys 1997;35:2093.
[12] Jourdan C, Cavaillé JY, Perez J. Polym Eng Sci 1988;28:1318.
[13] Cavaillé JY, Vassoile R, Thollet G, Rios L, Pichot C. Colloid Polym Sci 1991;269:248.
[14] Brodnyan JG, Konen T. J Appl Polym Sci 1964;8:687.
[15] Eckersley ST, Rudin A. J Coat Technol 1990;62:89.
[16] Jensen DP, Morgan LW. J Appl Polym Sci 1991;42:2845.
[17] Wang Y, Juhue D, Winnik MA, Leung OM, Goh MC. Langmuir 1992; 8:760.
[18] Goh MC, Juhue D, Leung OM, Wang YC, Winnik MA. Langmuir 1993;9:1319.
[19] Richard J. Polym Eng Sci 1993;34:3823.
[20] Nemirovski N, Narkis M. ACS Adv Chem Ser 1994;239:353.
[21] Chevalier Y, Hidalgo M, Cavaillé J.-Y, Cabane B. PMSE Symposium on latex film formation, Chicago 1995;73:95.
[22] Feng J, Winnik MA, Shivers RR, Clubb B. Macromolecules 1995;28: 7671.
[23] Goudy A, Gee ML, Biggs S, Underwood S. Langmuir 1995;11:4454.
[24] Gerharz B, Butt HJ, Momper B. Prog Colloid Polym Sci 1996;100:91.
[25] Patel AA, Feng J, Winnik MA, Vancso GJ, McBain CBD. Polym Eng Sci 1996;37:2277.
[26] Peters ACIA, Overbeek GC, Buckmann AJP, Padget JC, Annable T. Prog Org Coat 1996;29:183.
[27] Eckersley ST, Helmer BJ. J Coat Technol 1997;69:97.
[28] Winnik MA. In: Lovell PA, El-Aasser MS, editors. Emulsion polymerization and emulsion polymers. New York: Wiley; 1997. p. 468.
[29] Feng J, Odrobina E, Winnik MA. Macromolecules 1998;31:5290.
[30] Agarwal N, Farris RJ. J Appl Polym Sci 1999;72:1407.
[31] Chevalier Y, Hidalgo M, Cavaillé J-Y, Cabane B. Macromolecules 1999;32:7887.
[32] Haba Y, Segal E, Narkis M, Titelman GI, Siegmann A. Synth Met 2000;110:189.
[33] Robeson LM, Vratsanos MS. Macromol Symp 2000;155:117.
[34] Tzitzinou A, Keddie JL, Geurts JM, Peters ACIA, Satguru R. Macromolecules 2000;33:2695.
[35] Odrobina E, Feng J, Pham HH, Winnik MA. Macromolecules 2001; 34:6039.
[36] Robeson LM, Berner RA. J Polym Sci, Part B: Polym Phys 2001;39: 1093.
[37] Vorobyova O, Winnik MA. Macromolecules 2001;34:2298.
[38] Colombini D, Hassander H, Karlsson OJ, Maurer FHJ. J Polym Sci Polym Phys 2004 [in press].
[39] Colombini D, Hassander H, Karlsson OJ, Maurer FHJ. Macromolecules 2004;37:6865.
[40] Colombini D, Merle G, Alberola ND. J Appl Polym Sci 2000;76:530.
[41] Ljungberg N, Wesslén B. Polymer 2003;44(25):7679.
[42] Colombini D, Merle G, Alberola ND. Macromolecules 2001;34:5916.
[43] Colombini D, Maurer FHJ. Macromolecules 2002;35:5891.
[44] Colombini D, Maurer FHJ. Macromol Symposia 2003;198:83.
[45] Chern C-S, Poehlein GW. J Polym Sci, Part A: Polym Chem 1987;25: 617.
[46] Chern C-S, Poehlein GW. J Polym Sci, Part A: Polym Chem 1990;28: 3055.
[47] De la Cal JC, Urzay R, Zamora A, Forcada J, Asua JM. J Polym Sci, Part A: Polym Chem 1990;28:1011.
[48] Gilbert RG. Emulsion polymerization. A mechanistic approach. London: Academic Press; 1995.
[49] Mills MF, Gilbert RG, Napper DH. Macromolecules 1990;23:4247.
[50] Stubbs JM, Karlsson OJ, Jönsson J-E, Sundberg E, Durant Y, Sundberg DC. Colloids Surf, A 1999;153:255.
[51] Krywko WP, McAuley KB, Cunningham MF. Polym React Eng 2002; 10:135.
[52] Zeaiter J, Romagnoli JA, Barton GW, Gomes VG, Hawkett BS, Gilbert RG. Chem Eng Sci 2002;57:2955.
[53] Stubbs JM, Carrier R, Karlsson OJ, Sundberg DC. Prog Colloid Polym Sci 2003;124:131.
[54] Karlsson OJ, Stubbs JM, Carrier RH, Sundberg DC. Polym React Eng 2003;11:589.
[55] Berg J, Sundberg DC, Kronberg B. Polym Mater Sci Eng 1986;54: 367.
[56] Sundberg DC, Casacca AP, Pantazopoulos J, Muscato MR, Kronberg B, Berg J. J Appl Polym Sci 1990;41:1425.
[57] Chen YC, Dimonie V, El-Aasser MS. J Appl Polym Sci 1991;42(4): 1049.
[58] Okubo M, Katsuta Y, Matsumoto T. J Polym Sci: Polym Lett Ed 1980; 18:481.
[59] Lee DI. ACS Symposium Series, Washington DC; 1981; 165:405.
[60] Cho I, Lee K-W. J Appl Polym Sci 1985;30:1903.
[61] Jönsson J-E, Hassander H, Jansson LH, Törnell B. Macromolecules 1991;24:126.
[62] Lee S, Rudin A. J Polym Sci, Part A: Polym Chem 1992;30:2211.
[63] Karlsson O, Hassander H, Wesslen B. J Appl Polym Sci 1997;63: 1543.
[64] Dimone VL, Daniels ES, Shaffer OL, El-Aasser MS. In: Lovell PA, El-Aasser MS, editors. Emulsion polymerization and emulsion polymers. New York: Wiley; 1997. p. 293.
[65] Sundberg DC, Durant YG. In: Asua JM, editor. Polymeric dispersions: principles and applications. London: Kluwer; 1997. p. 155.
[66] Karlsson OJ, Sundberg DC. In: recent research developments in macromolecules research. Trivandrum, India: Research Signpost; 1998 p. 325.
[67] Sundberg DC, Durant YG. Polym React Eng 2003;11:379.
[68] Thompson EV. J Polym Sci, Part B: Polym Phys 1965;3:675.
[69] Talmon Y. Proceedings of the Annual Meeting—Electron Microscopy Society of America (EMSA) 1987;496.
[70] Karlsson OJ, Hassander H, Colombini D. C R Chemie 2003;6:1233.
[71] Karlsson OJ, Stubbs J, Karlsson LE, Sundberg DC. Polymer 2001;42: 4915.
[72] Durant YG, Carrier RH, Sundberg DC. Polym React Eng 2003;11: 433.

[73] Ivarsson LE, Karlsson OJ, Sundberg DC. Macromol Symp 2000;151:407.
[74] Stubbs JM, Sundberg DC. J Coat Technol 2003;75(938):59.
[75] Karlsson LE, Karlsson OJ, Sundberg DC. J Appl Polym Sci 2003;90:905.
[76] Stubbs JM, Sundberg DC. J Appl Polym Sci 2004;91(3):1538.
[77] Piton MC, Gilbert RG, Chapman BE, Kuchel PW. Macromolecules 1993;26:4472.
[78] Tonge MP, Stubbs JM, Sundberg DC, Gilbert RG. Polym Eng Sci 2000;41:3659.
[79] Tonge MP, Gilbert RG. Polym Eng Sci 2001;42:501.
[80] Russel DT, Gilbert RG, Napper DH. Macromolecules 1992;25:2459.
[81] Russel DT, Gilbert RG, Napper DH. Macromolecules 1993;26:3538.
[82] Davis TP, O'Driscoll KF, Piton MC, Winnik MA. J Polym Sci, Part C: Polym Lett 1989;27:181.
[83] Tefera N, Weickert G, Westerterp KR. J Appl Polym Sci 1997;63:1663.
[84] Lovell PA, Shah TH, Heatley F. Polym Mater Sci Eng 1991;64:278.
[85] Britton D, Heatley F, Lovell PA. Macromolecules 2000;33:5048.
[86] Ahmad NM, Lovell PA, Heatley F. Polym Prepr (ACS Div of Polym Chem) 2002;43:652.
[87] Britton D, Heatley F, Lovell PA. Macromolecules 1998;31:2828.
[88] Ahmad NM, Heatley F, Lovell PA. Macromolecules 1998;31:2822.
[89] Stubbs JM, Durant YG, Sundberg DC. C R Chemie 2003;6:1217.